ELSEVIER

Chemical Engineering Journal 130 (2007) 19–28

Chemical Engineering Journal

www.elsevier.com/locate/cej

Dynamic modeling of batch polymerization reactors via the hybrid neural-network rate-function approach

Jyh-Shyong Chang *, Shih-Chieh Lu, Yu-Lun Chiu

Department of Chemical Engineering, Tatung University, 40 Chungshan North Road, 3rd Sec., Taipei, Taiwan, ROC

Received 16 May 2006; received in revised form 6 November 2006; accepted 21 November 2006

Abstract

A simulated verification and validation of the hybrid neural-network rate-function (HNNRF) approach to modeling batch reactor systems is provided. In chemical reactor processes, some measurements may not be easily obtainable, and the designed neural-network rate-function (NNRF) model in our previous work did not propose a method to include the state variables for the suggested dynamic model. To overcome this difficulty, the approximated mechanistic equations characterizing these immeasurable state variables could be incorporated into the NNRF model to form the hybrid neural-network rate-function model. The sequential pseudo-uniform design (SPUD) is used to locate the sufficient but limited experiments to provide the HNNRF model with rich information. In this research, the HNNRF modeling capability over a large operating region was evaluated employing a simulated polymerization reactor system. In addition to the comparative benefit of short time expenditure for building the model, the performance of the identified HNNRF model is quite acceptable in the face of noisy measurements and the identified model could be applied to determine the optimal recipe or the operating conditions of the reactor systems.

Keywords: Neural networks; Batch reactor; Polymerization; Uniform design

1. Introduction

Effective control, optimization, or monitoring of a process needs an accurate model characterizing the nonlinear dynamic behavior. These targets may be achievable through a reliable process model formulated classically on the basis of mass and energy balance for chemical processes [1,2]. When one is to construct a mechanistic model for a batch or semibatch reactor system, the most challenging difficulties are to determine the reaction rates of the reaction system by proposing a suitable reaction laws and estimating the uncorrelated parameters used in the proposed rate laws. Generally, the mathematical expressions describing the rate laws as a function of the variables are unknown. In contrast, if these expressions are available, the unknown parameters have to be fitted employing nonlinear optimization techniques and the correlated parameters are usually estimated [3]. In order to overcome these difficulties, neural networks have been utilized as an alternative to the traditional mathematical models to simulate nonlinear patterns [4]. Development of a neural wok model demands less time than that needs on the basis of traditional mathematical models because a systematic approach is usually provided.

The conventionally adopted architecture of artificial neural networks (ANNs) for process modeling is the layered feedforward artificial neural networks (FANNs) [5,6]. Before a neural network is applied to a set of data for obtaining a data-driven model, factors such as the topology of the network, along with the measure of the causal importance of individual input variables [7,8], must be taken into account. Hybrid neural network first principles architecture is an alternative neural network modeling approach that can be found in the literature [9–13]. The hybrid model combines a partial first principles model, which incorporates the then available knowledge about the process being modeled into a neural network that serves as an estimator of unmeasured process parameters difficult to be determined from first principles. This hybrid model has better properties than standard black-box neural network models in that it is

Abbreviations: AIBN, azobis(isobutyronitrile); ANN, artificial neural network; FANN, feedforward neural networks; FD, factorial design; HNNRF, hybrid neural-network rate-function; MMA, methyl methacrylate; MSE, mean squared error; NNPF, neural-network parameter-function; NNRF, neural-network rate-function; SPUD, sequential pseudo-uniform design; UD, uniform design

* Corresponding author. Tel.: +886 2 5925252 2561; fax: +886 2 5861939.
E-mail address: jschang@ttu.edu.tw (J.-S. Chang).

1385-8947/$ – see front matter © 2006 Elsevier B.V. All rights reserved.
doi:10.1016/j.cej.2006.11.011

Nomenclature

0	initial
a	curve fitting parameter
E	activation energy (kJ/(kmol K))
f	nonlinear function
g	function for curve fitting
h	measurement function
HI	polydispersity
I	initiator
J	sensitivity information value
k_d	rate constant for the initiator decomposition reaction (s^{-1})
M	monomer molecular
$\bar{M}_n$	number average molecular weight of polymerization (kg/kmol)
n	the dimension of the recurrent states
n_m	number of measurements during a batch operation
n_t	number of total batches
n_s	number of samples
P_N	number-average degree of polymerization
t	time (s)
t_f	final reaction time for polymerization reaction (s)
T	temperature (°C)
U	uniform design
$U_n(n^s)$	UD with s control facors and n levels partitioned in each control factor; a total of n experiments are designed
$\text{SPUD}_m((m+n)^s)$	SPUD with s control facors and $m+n$ levels partitioned in each control factor (followed the $U_n(n^s)$ design); a total of m experiments are designed
u	external input
V	volume of reacting mixture (m^3)
W	weight (kg)
x	input vector of FANN model
$\boldsymbol{x}'$	scaled input of FANN model
$\dot{\boldsymbol{x}}'$	scaled output of FANN model
$\boldsymbol{x}$	the vector of n variables
X	conversion of monomer
$\boldsymbol{y}$	process measurements
$\boldsymbol{y}'$	scaled process measurements
$\widehat{\boldsymbol{y}}$	model output
$\widehat{\boldsymbol{y}}'$	scaled model output
[]	molar concentration (kmol/m^3)

Greek letters

$\lambda_i\|_{i=0,1,2}$	ith moment of living radical distribution
$\mu_i\|_{i=0,1,2}$	ith moment of dead polymer distribution
σ	measurement noise

Superscript

^	estimated quantity
*	optimal

Subscripts

0	initial
d	decomposition
i	initial
M	monomer
n	number of experimental trials for FD/UD/SPUD method
s	solvent

able to interpolate and extrapolate much more accurately, is easier to analyze and interpret, and requires significantly fewer training examples. The motivation of the studies [12,13] arose from the fact that biotechnological reactions are difficult to model, with reaction mechanisms still unknown and the reaction order yet to be postulated and experimentally verified. The resulting fundamental model is only as good as the postulated functional form in the model. Neural networks, which are universal-function approximators, can instead be used to learn the parameter functions in dynamic models. Thus, the adoption of prior process knowledge (usually in the form of conservation equations) coupled with the approximation capabilities of neural networks constitutes the neural-network parameter-function (NNPF) modeling approach.

Although the NNPF modeling approach had been verified experimentally, with only two unknown parameters involved in the dynamic equations, the reactor system studied in the works of Tholudur and Ramirez [12,13] was rather simple. Similar case studies with limited parameters can be found in the works cited [9,10] in developing the hybrid neural-network first principles approach. In case of the free radical polymerization reaction of methyl methacrylate (MMA) [1,14], there are more than 12 parameters involved. Direct application of NNPF modeling approach or hybrid modeling approach to the polymerization reaction system will be restricted. Chang and Hung [15] proposed the neural-network rate-function (NNRF) modeling approach to obtain a reliable dynamic neural network model characterizing the complex MMA polymerization reactions carried out in a batch reactor. In the proposed NNRF modeling approach, the rate change of the states as a function of the selected states could be built directly by an FANN for an unknown process. In this way, the postulated functional forms in the NNPF model will no longer be required. The predictive capa-

Table 1
MSE of the identified HNNRF model based on the data collected from different design of experiments

Design of experiments	MSE for the recall	MSE for the testing
$FD_8(2^3)$ (8 batches)	0.333	249.032
$(U_8(8^3)$ (8 batches)	0.158	0.254
$SPUD_7(15^3)$ (15 batches)[a]	0.160	0.169
$SPUD_7(15^3)$ (15 batches)[b]	0.160	0.192
$SPUD_7(15^3)$ (15 batches)[c]	0.523	4.274

[a] Adopting [I] and μ_1 as the recurrent states.
[b] Adopting [I] and X as the recurrent states.
[c] Adopting [I], μ_1, and X as the recurrent states.

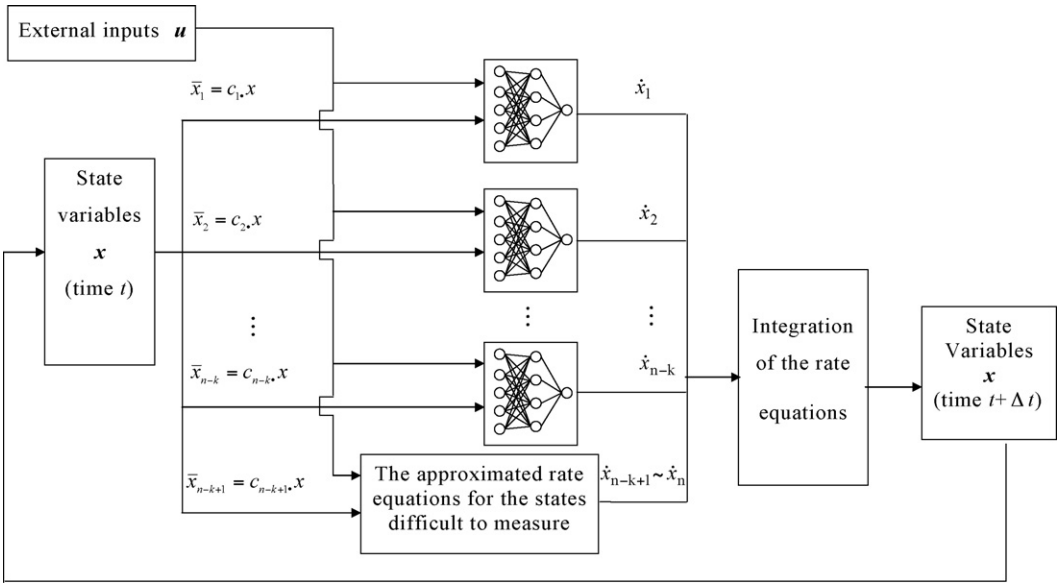

Fig. 1. Schematic diagram of hybrid neural-network rate-function (HNNRF) model.

bility of the NNRF model was found to be acceptable and optimal temperature trajectories were calculated accordingly [15]. However, the NNRF model developed [15] was built only on the measurable states. It did not include the state variables difficult to measure, among which was the initiator concentration during the polymerization reaction. Therefore, in this work, we will extend the modeling methodology of Chang and Hung [15] and propose the hybrid neural-network rate-function (HNNRF) modeling approach to tackle this problem, which is usually encountered in complex reactor systems. In addition, both the way to measure the causal importance of individual input variables and the computational algorithm to cope with the noisy measurements in building the NNRF or HNNRF model are also addressed in this work.

2. Simulation of the batch polymerization reactor

To demonstrate the applicability of the proposed HNNRF modeling approach, free radical solution polymerization reactions of MMA in a batch reactor were simulated as a testing process. Model equations for batch MMA polymerization reactions and the related kinetic parameters can be found in the literature [1,14–16]. Especially, one can find the details of mathematical description of MMA solution polymerization batch reactor in the appendix of Chang and Hung [15]. The loading conditions (W_M (MMA) = 3.492 kg; W_s (toluene) = 5.239 kg; [I] (AIBN) = 0.05–0.1 mol/dm^3) were used in this study.

Table 2
The relationship between the available measurements and the derived measurements

Available measurements	Derived measurements
$X^*(t_f)$	$\mu^*_{0f} \equiv \frac{V(0)[M(0)]X^*(t_f)}{P^*_N(t_f)}$
$P_N{}^*(t_f)$	$\mu^*_{1f} \equiv V(0)[M(0)]X^*(t_f)$
$HI^*(t_f)$	$\mu^*_{2f} \equiv V(0)[M(0)]X^*(t_f)P^*_N(t_f)HI^*(t_f)$

3. Hybrid neural-network rate-function model

Development of the hybrid neural-network rate-function (HNNRF) model for nonlinear dynamic systems is based on the developed NNRF model (NNRF) [15]. In developing the NNRF or HNNRF model, the differential equations governing the dynamic behavior of a nonlinear process are represented as

$$\begin{aligned} \dot{x}_{i=1-n} &= f_{i=1-n}(\bar{\boldsymbol{x}}_i, \boldsymbol{u}) \\ \bar{\boldsymbol{x}}_i &= \boldsymbol{c}_i \cdot \boldsymbol{x} \\ \hat{\boldsymbol{y}} &= \boldsymbol{h}(\boldsymbol{x}) \end{aligned} \tag{1}$$

where $x_{i=1-n}$ are the elements of the state variables $\boldsymbol{x}$, $f_{i=1-n}$ rate functions, $\boldsymbol{u}$ external inputs, and $\boldsymbol{c}_i \cdot \boldsymbol{x}$ is the array multiplication

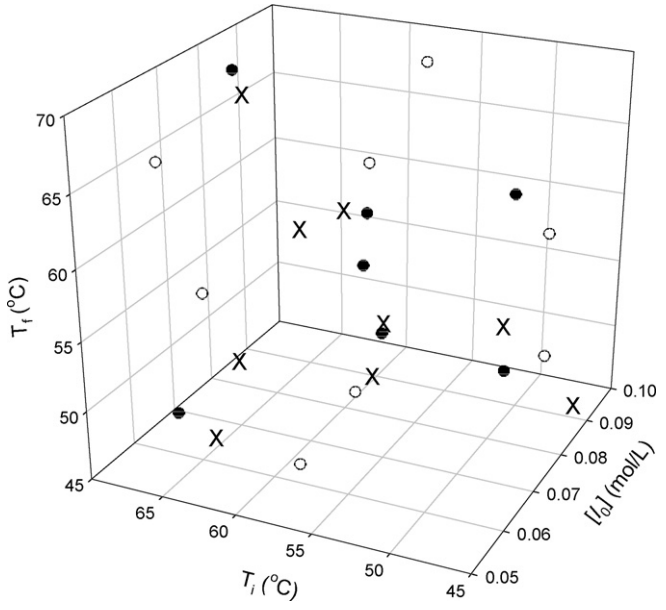

Fig. 2. The design of experiments based on the UD and SPUD, and the testing data sets ((◯) $U_8(8^3)$; (●) $SPUD_7(15^3)$; (×) testing data sets).

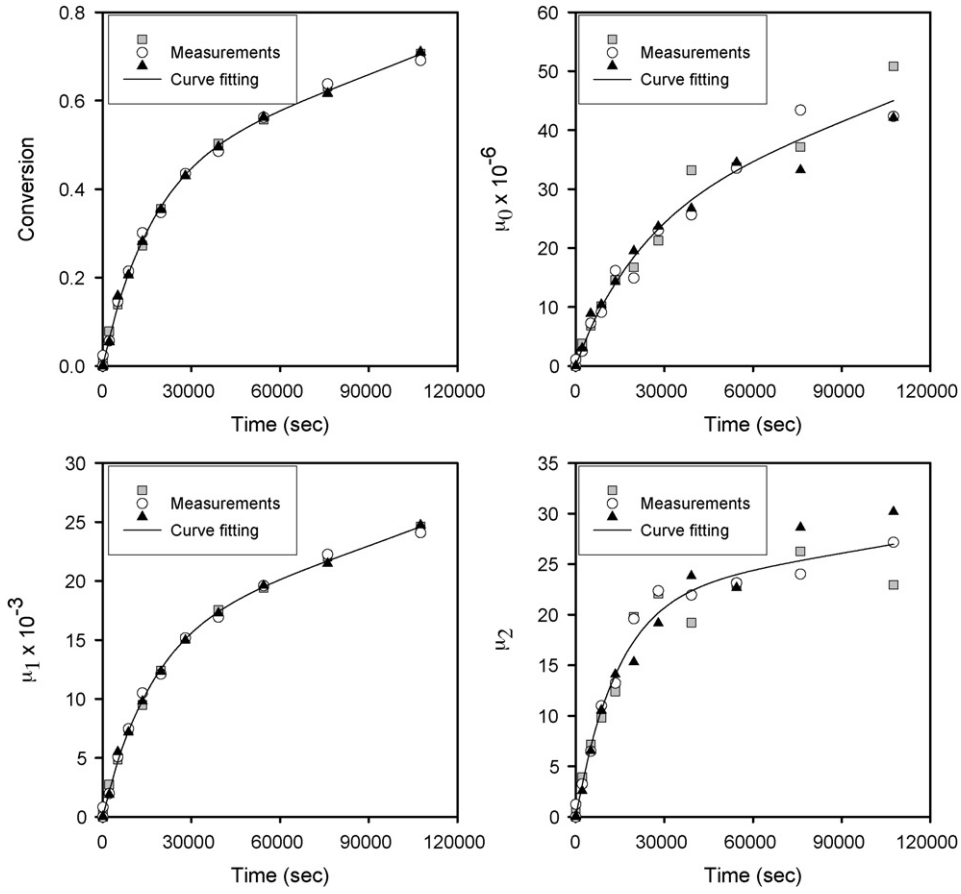

Fig. 3. Curve fitting of the states X, μ_0, μ_1, and μ_2 for one of the experiments.

of $\boldsymbol{c}_i$ and $\boldsymbol{x}$. The vector $\boldsymbol{c}_i$ is a vector whose element is either zero or one.

Many studies have proven the capability of FANNs to approximate any nonlinear relationship between a set of inputs and outputs [9,17,18]. An FANN can be applied to construct a mapping between inputs $\boldsymbol{x}$ and outputs $\boldsymbol{y}$ of a system without discovering the physical relationship between inputs and outputs. If the inputs $\boldsymbol{x}$ are selected to be the measurable state variables and the outputs $\boldsymbol{y}$ the rates of the corresponding measurable state variables, the constructed FANN can be embedded in the dynamic equations governing the measurable state variables to obtain the dynamic behavior of the state variables. According to this approach, the NNRF model can be constructed for a complex reaction system [15]. In contrast, if the dynamic behavior of some state variables that are difficult to measure may be described by the approximate mechanistic equations if they are available. Combination of a completely black-box model (NNRF model adopted here) with approximate mechanistic equations could construct the so-called HNNRF model (Fig. 1). Although it seems that the extension of the NNRF model to the HNNRF model is straightforward and simple, the capability of the HNNRF modeling approach investigated in this work proposes an approach to obtain a reliable dynamic model over a broad operating region from the accessible data for real complex batch reaction processes without resorting to complex mathematical manipulations.

3.1. Derivative estimation of state variables

When one applies the NNRF or HNNRF modeling approach to an unknown process, the rates of states from the available measurements are needed. In the face of noise-corrupted measurements, a collection of time dependent experimental data $y(t)$ is assumed to be located along a state trajectory $\hat{x} = g_j(t)$ characterized by one of the following functions:

$$g_1 = a_1\ \mathrm{e}^{a_3 t} + a_2\ \mathrm{e}^{a_4 t} \tag{2}$$

$$g_2 = \frac{1}{a_1 + a_2 t} \tag{3}$$

$$g_3 = a_1 + a_2 t + a_3 t^2 + a_4 t^3 \tag{4}$$

$$g_4 = \frac{t}{a_1 + a_2 t} \tag{5}$$

$$g_5 = \frac{a_1}{(1 + \mathrm{e}^{-a_2(t-a_3)})} + a_4 \tag{6}$$

$$g_6 = a_1 t^{a_2} \tag{7}$$

The forms of these profiles are possible patterns for the dynamic experimental data usually encountered in batch processes. More functional form of $\hat{x} = g(t)$ could be found in the work of Edgar and Himmelblau [19] and adopted as a potential candidate. Estimation of the parameters in a selected function for

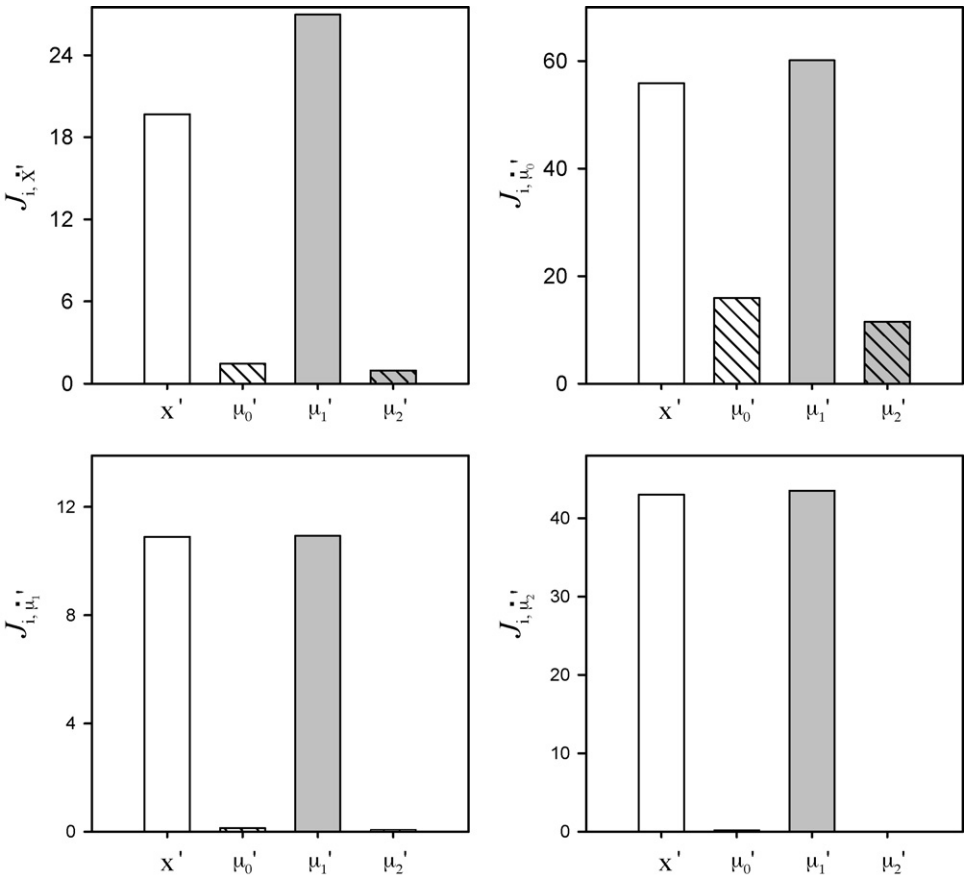

Fig. 4. The sensitivity information values with respect to X, μ_0, μ_1, μ_2 (Eq. (9)) calculated for the eight batches ($U_8(8^3)$).

curve fitting of the experimental data is achieved by the following minimization problem:

Objective

$$\underset{i=1\sim 6}{\text{Min}}\left[\underset{a_1\sim a_4}{\text{Min}}\sum_{j=1}^{m}(y_j - g_{ij})^2\right] \tag{8}$$

Once a function representing the data points is obtained using the above nonlinear programming, the derivative of this function can be calculated analytically or numerically to obtain the derivative of the measurable state variables $\dot{x}_{i=1-n}$.

3.2. Neural network training

Once the rates of states are estimated, they could be related to the external inputs and the recurrent states via FANNs. For FANN training, appropriate selection of the inputs including the external inputs and the recurrent states is very important to assure the performance of the identified NNRF or HNNRF model. The neural network models represent a powerful tool for complicated process identification. However, because they belong to the category of data-driven "black box" models, they cannot avoid the consequences of the "garbage in–garbage out" rule [8]. Instead of applying the information theoretic subset selection (ITSS) method to select appropriate subsets of inputs for FANN model development [7,8], the following sensitivity information value estimated directly on the basis of the identified FANNs could be used to rate the relevance of the input variables to an output variable:

$$J_{i,j} = \sum_{l=1}^{n_t}\int_{t_0}^{t_f}\frac{\partial \dot{x}_i'}{\partial x_j'}\,\mathrm{d}t \tag{9}$$

A larger value of $J_{i,j}$ will characterize the scaled input x_j' containing more information relevant to the desired FANN mapping between the scaled input x_j' and the scaled output x_i' for all the n_t batches. Computer experiments adopting the significant input variables, appropriate hidden nodes of an FANN in the HNNRF model, and appropriate training epochs could achieve an acceptable identified HNNRF model. The input and output data are scaled for training by the following equation:

$$x_i' = 0.9\left(\frac{x_i - x_{i,\min}}{x_{i,\max} - x_{i,\min}}\right) + 0.05 \tag{10}$$

The performance of an identified HNNRF model is estimated on the basis of the mean squared error (MSE) between the scaled fitted measurements and the scaled model outputs calculated using all the measurements in the recalled data sets and the testing data sets, respectively, according to:

$$\text{MSE} = \frac{\sum_{i=1}^{n_t}\sum_{j=1}^{n_m}\sum_{k=1}^{n_s}(y_{ijk}' - \hat{y}_{ijk}')^2}{n_t} \tag{11}$$

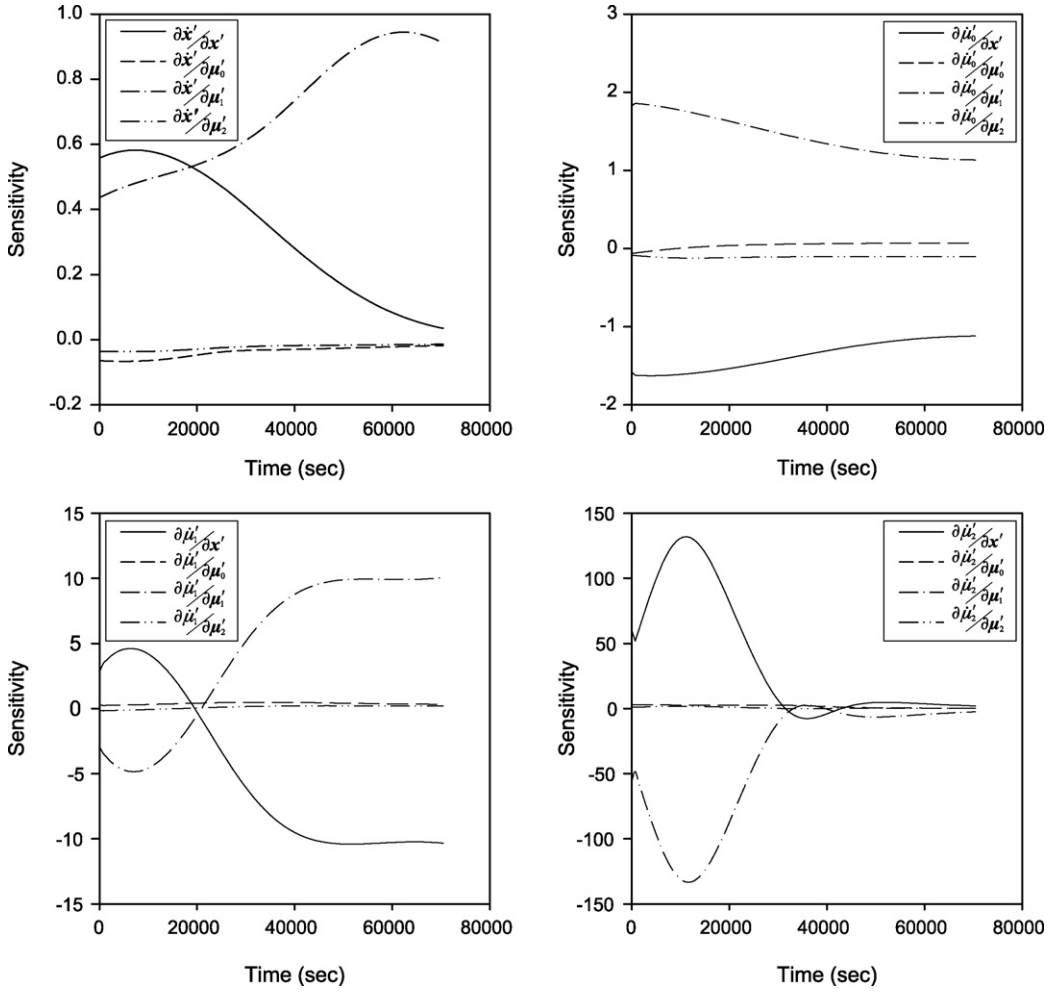

Fig. 5. The time profiles of the output sensitivity wit respect to inputs (the FANNs shown in Table 3).

To provide an identified HNNRF model with rich information, the developed sequential pseudo-uniform design (SPUD) method [20] will be applied to locate limited but sufficient experiments for gathering the experimental data. The developed SPUD method is an extended version of the uniform design (UD) method [21]. With respect to the detail of the SPUD method, one could make reference to our previous work [20]. In this work, the experiments for gathering the training data based on the UD method will be performed at first. If the data are not enough, the further experiments located by the SPUD method will provide the HNNRF identification with further information. The additional experiments located around the interpolated spatial locations of the experiments for gathering the training data sets will be used as the validation data sets.

4. HNNRF model development for the batch polymerization reactor

Because the concentration of the initiator is difficult to measure, an identified NNRF model governing the major state variables of this polymerization reaction system can be combined with the approximate mechanistic equation (Eq. (12)), which describes the dynamic behavior of the initiator to establish the HNNRF model for the MMA polymerization reaction system:

$$\frac{\mathrm{d[I]}}{\mathrm{d}t} = -k'_{\mathrm{d}}\,[\mathrm{I}] \tag{12}$$

Table 3
The constructed FANNs in the HNNRF model using $FD_8(2^3)$ and $U_8(8^3)$ experimental data, respectively

FANN	Output	External input	Recurrent states	Number of hidden nodes	Transfer function used (first layer)	Transfer function used (second layer)
#1	$\dot{X}$	T	[I], μ_1	7	Log-sigmoid	Linear
#2	$\dot{\mu}_0$	T	[I], μ_1	2	Log-sigmoid	Linear
#3	$\dot{\mu}_1$	T	[I], μ_1	2	Log-sigmoid	Linear
#4	$\dot{\mu}_2$	T	[I], μ_1	3	Log-sigmoid	Linear

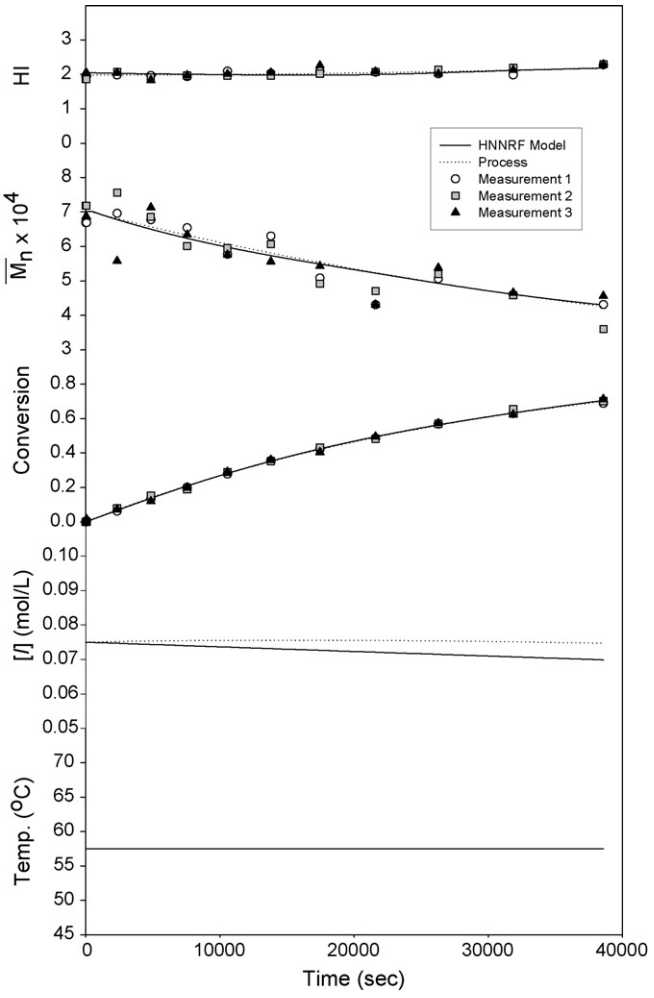

Fig. 6. Comparison of the states generated from the identified HNNRF model (Table 4) and the process for one of the recalled experiments (a constant temperature profile).

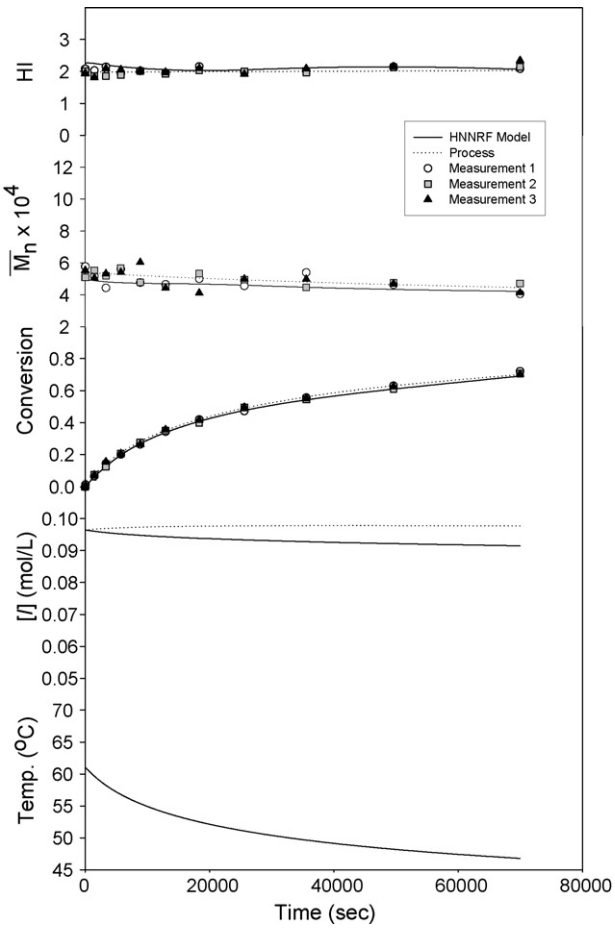

Fig. 7. Comparison of the states generated from the identified HNNRF model (Table 4) and the process for one of the recalled experiments (an exponential decay temperature profile).

In the above equation, $k'_{d0} = 0.7k_{d0}$ and $E'_d = 0.994E_d$ were assumed.

To provide the identified HNNRF model with rich information, the experiment design methods ($U_8(8^3)$ and $SPUD_7(15^3)$ shown in the first column of Table 1) were performed. The control factors and the range of each control factor used in this case study are the initial and final temperatures T_i, T_f of the designed temperature trajectories (45–70 °C) and the initial initiator concentration $[I]_0$ (0.05–0.1 mol/dm^3). The external input (temperature trajectory) was designed as:

$$T(t) = \frac{X(t)}{X_f}(T_f - T_i) + T_i \tag{13}$$

A spatial plot of the experimental locations in terms of these three control factors designed by the UD (symbol '◯') followed by the SPUD (symbol '●') is shown in Fig. 2. The additional nine experimental locations indicated by symbol '×' in the same figure are arranged for assessing the identified HNNRF model. For demonstration of the applicability of the proposed HNNRF modeling approach to the process in which some states are not easily achievable, the testing batches consist of varied doses of the initiator loading as shown in Fig. 2. In order to examine the performance of the identified HNNRF model confronted with conventional temperature trajectories employed in a batch operation, there are two more testing experiments along the designed temperature trajectories as to be exhibited in Figs. 9 and 10. Furthermore, to ascertain that the UD or

Table 4
The constructed FANNs in the HNNRF model using $U_8(8^3) + SPUD_7(15^3)$ experimental data

FANN	Output	External input	Recurrent states	Number of hidden nodes	Transfer function used (first layer)	Transfer function used (second layer)
#1	$\dot{X}$	T	[I], μ_1	10	Log-sigmoid	Linear
#2	$\dot{\mu}_0$	T	[I], μ_1	2	Log-sigmoid	Linear
#3	$\dot{\mu}_1$	T	[I], μ_1	2	Log-sigmoid	Linear
#4	$\dot{\mu}_2$	T	[I], μ_1	2	Log-sigmoid	Linear

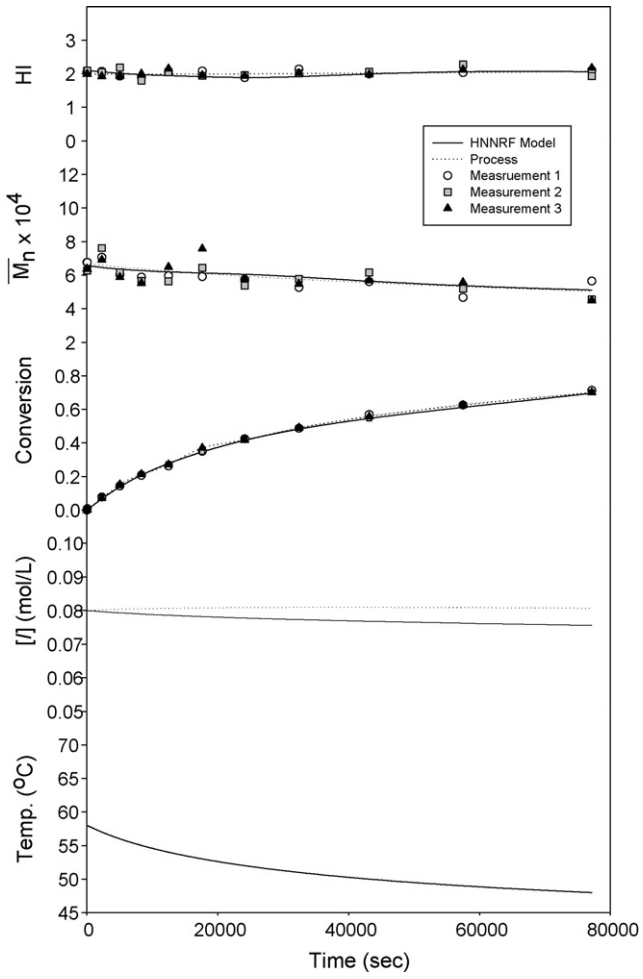

Fig. 8. Comparison of the states generated from the identified HNNRF model (Table 4) and the process for one of the testing experiments (an exponential decay temperature profile).

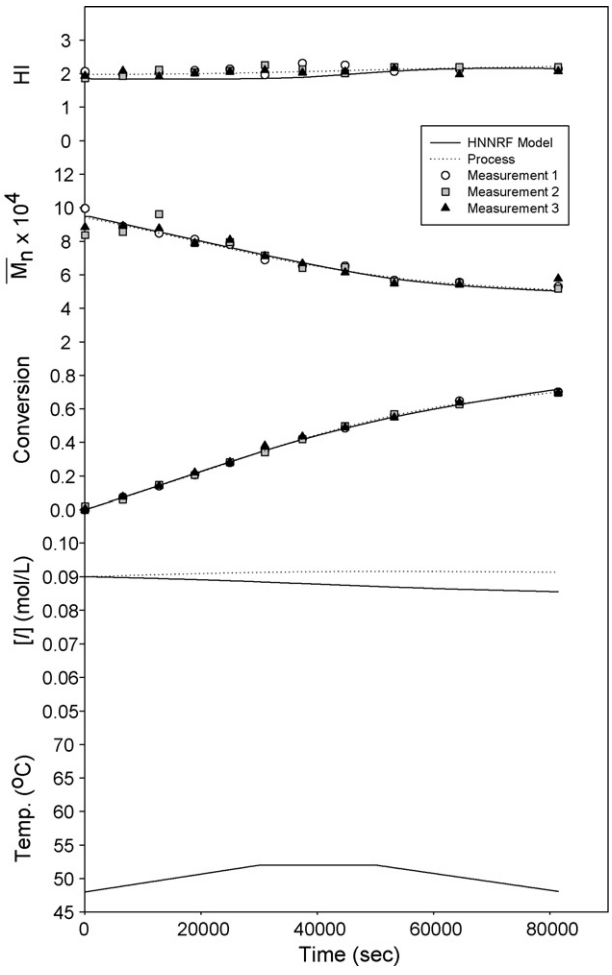

Fig. 9. Comparison of the states generated from the identified HNNRF model (Table 4) and the process for one of the testing experiments (a traditional heating, reacting and cooling temperature profile).

SPUD method could provide us with more information about the unknown process, the 2^3 factorial design $FD_8(2^3)$ experiments were also performed for comparison (Table 1). The measurement noise for X, HI, and $\bar{M}_n$ was assumed to be $\sigma_X = 0.01$, $\sigma_{HI} = 0.1$, and $\sigma_{\bar{M}_n} = 5000$ kg/kmol, respectively, according to our previous experimental work [22]. The eight batches ($U_8(8^3)$) with repeated measurements at the sampling time (symbols shown in Fig. 2) were first employed for constructing the HNNRF model. The available measurements were X, $\bar{M}_n$, and HI. The derived measurements X, μ_0, μ_1, and μ_2 can be obtained based on the equations given in Table 2. Applying the method of obtaining the derivatives of state variables to this case study, the states X, μ_0, μ_1, and μ_2 are properly fitted to one of the Eqs. (2)–(7) and are shown in Fig. 3. The rate changes of X, μ_0, μ_1, and μ_2 were computed using the fitted curve. Adopting 80 data points of the fitted T, [I], X, μ_0, μ_1, μ_2 as the inputs and one of the corresponding rate changes of X, μ_0, μ_1, and μ_2 as the output for each batch, four FANNs were well trained and the sensitivity information values with respect to X, μ_0, μ_1, μ_2 (Eq. (9)) were calculated for these eight batches (Fig. 4). Because T is the external input and [I] is the desired recurrent state, these two inputs were consequently not considered in the calculation of the sensitivity information values. One of the sensitivity profiles for the FANN characterizing the inputs and the output is shown in Fig. 5. Based on Fig. 4, we can select appropriate subsets of inputs for constructing these four FANNs to be embedded in the HNNRF model. Possible choices of relevant inputs for all the FANNs are (T, [I], μ_1), (T, [I], X), and (T, [I], μ_1, X).

The identified HNNRF models (Table 3) on the basis of the available data sets ($FD_8(2^3)$ and $U_8(8^3)$ in Table 1, respectively) are summarized in columns two and three as shown in Table 1. There is a small difference in the MSE value between these two methods for the recalled sets but a larger discrepancy exists for the testing sets. This indicates the advantage of the UD method over the FD method in providing the HNNRF model with the dynamic information given the same batches. One possible reason is that there are eight levels utilized in each control factor designed by the UD method as opposed to three levels used in the FD method. From the data shown in Table 1, the identified HNNRF model appears to be acceptable in the recalled sets (MSE = 0.158) and the testing sets (MSE = 0.254) if the experimental resources are limited. However, there exists potential improvement in the testing sets. Therefore, the data

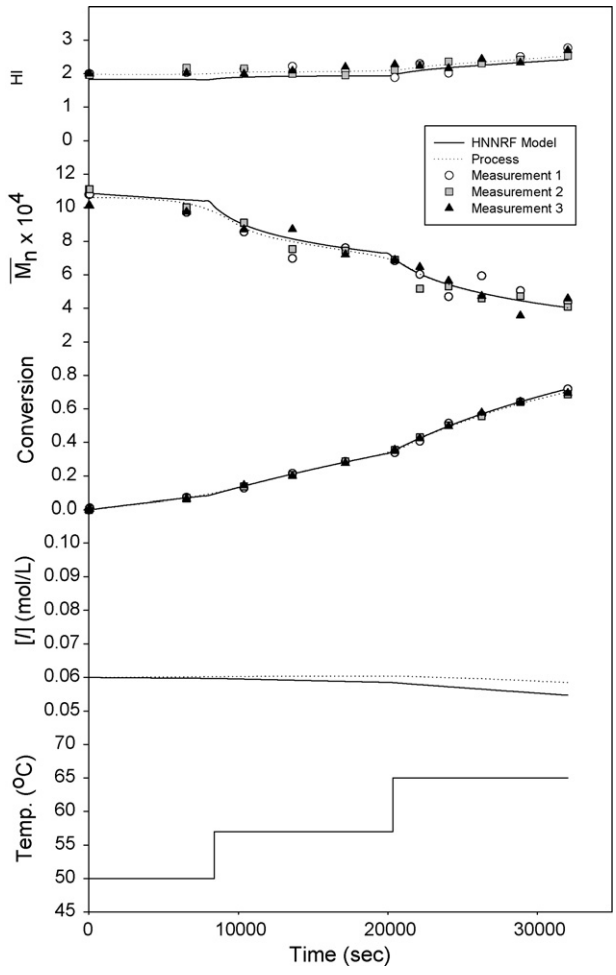

Fig. 10. Comparison of the states generated from the identified HNNRF model (Table 4) and the process for one of the testing experiments (a step-wise temperature profile).

of the additional seven batches designed via the SPUD method (Fig. 2) combined with the previous eight batches were used to construct another HNNRF model (Table 4). One can find that the generalization of the identified HNNRF model for the testing set is really improved (the MSE is reduced from 0.254 to 0.169) as shown in Table 1. The performance of the identified HNNRF model (Table 4) for the recalled sets are shown in Figs. 6 and 7 while those for the testing sets are shown in Figs. 8–10. These five figures are used only for illustration. The results for both the recalled sets and the testing sets are acceptable in spite of the trajectory discrepancies in the initiator concentration between the process and the model shown in these figures. This verifies that the main objective of this work is achieved. The HNNRF model extends the capability of the NNRF model [15] to the process in which some states are not easily achievable.

The other potential choices of relevant inputs for all the FANNs are (T, [I], X), and (T, [I], μ_1, X). As shown in Table 1, the identified HNNRF model with the recurrent states T, [I], X performs comparably with that adopting the recurrent states T, [I], μ_1. For brevity, the figures for displaying the performance are left out. We also evaluated the performance of the HNNRF model on the basis of 15 batches and adopting T, [I], μ_1, X as the recurrent states, but no acceptable result was obtained (Table 1). This may be attributed to the fact that an excessive number of inputs were adopted to construct the FANNs.

5. Conclusions

Direction application of the NNRF model hinges on whether all the states of the process are measurable. Whereas the concentration of the initiator is difficult to measure during the polymerization of MMA, the NNRF model governing the major state variables of this polymerization reaction system could be combined with the approximate mechanistic model characterizing the reaction behavior of the initiator to establish the HNNRF model for the MMA polymerization reaction system.

To provide the identified HNNRF model with rich information, the UD method is much better than the conventional FD method given the same batches. A reliable HNNRF model with four FANNs was identified using 8 and 15 batches information, although the latter exhibited a better prediction capability. Facing the measurements corrupted with noise, the capability of the identified HNNRF model is quite acceptable. Furthermore, the appropriate input adoption of the FANNS plays an import role in constructing a reliable HNNRF model. The sensitivity information value estimated on the basis of the fitted experimental data can direct the user to choose relevant inputs. Once the HNNRF model is identified, it could be implemented to determine the optimal feed loadings and operating conditions of complex processes, which are difficult to be modeled by a mechanistic model employing the first principles.

Acknowledgments

We thank the National Science Council (Grant NSC 94-2214-E-036-003) and Dr. T.S. Lin, President of Tatung University, Taipei, Taiwan, for all the support conducive to the completion of this work

References

[1] S.R. Ponnuswamy, S.L. Shah, Ind. Eng. Chem. Res. 26 (1987) 2229.
[2] J.S. Chang, J.L. Lai, Ind. Eng. Chem. Res. 31 (1992) 861.
[3] J.R. Banga, K.J. Versyck, J.F.V. Impe, Ind. Eng. Chem. Res. 41 (2002) 2425.
[4] C. Shene, C. Diez, S. Bravo, Comput. Chem. Eng. 23 (1999) 1097.
[5] D.E. Rumelhart, G.E. Hinton, R.J. Williams, Nature 323 (1986) 533.
[6] J. Thibault, V.V. Breusegem, A. Chéruy, Biotechnol. Bioeng. 36 (1990) 1041.
[7] D.V. Sridhar, E.B. Bartlett, R.C. Seagrave, Comput. Chem. Eng. 22 (1998) 613.
[8] S. Papadokonstantakis, S. Machefer, K. Schnitzlein, A.I. Lygeros, Chem. Eng. 29 (2005) 1647.
[9] D.C. Psichogios, L.H. Ungar, AIChE J. 38 (1992) 1499.
[10] M.L. Thompson, M.A. Kramer, AIChE J. 40 (1994) 1328.
[11] Shene, C. Diez, S. Bravo, Comput. Chem. Eng. 23 (1999) 1097.
[12] A. Tholudur, W.F. Ramirez, Biotechnol. Prog. 12 (1996) 302.
[13] A. Tholudur, W.F. Ramirez, AIChE J. 45 (1999) 1660.
[14] P.E. Balliagou, D.S. Soong, Chem. Eng. Sci. 40 (1985) 75.
[15] J.S. Chang, B.C. Hung, Ind. Eng. Chem. Res. 41 (2002) 2716.

[16] P.E. Balliagou, D.S. Soong, Polym. Eng. Sci. 25 (1985) 212.
[17] J. Pollard, F. Broussard, M.R. Garrison, K.Y. San, Comput. Chem. Eng. 16 (1992) 253.
[18] I.M. Galvàn, J.M. Zaldivar, H. Hernandez, E.T. Molga, Comput. Chem. Eng. 20 (1996) 1451.
[19] T.F. Edgar, D.M. Himmelblau, Optimization of Chemical Processes, McGraw-Hill Inc., Singapore, 1989.
[20] J.S. Chang, J.P. Lin, Ind. Eng. Chem. Res. 43 (2004) 4278.
[21] Y.Z. Liang, K.T. Fang, Q.S. Xu, Chem. Int. Lab. Syst. (2001) 58.
[22] J.S. Chang, P.H. Liao, Ind. Eng. Chem. Res. 38 (1999) 144.